Probing Excitons in Ultrathin PbS Nanoplatelets with Enhanced Near-Infrared Emission

Manteiga Vázquez, Francisco; Yu, Qianli; Klepzig, Lars F.; Siebbeles, Laurens D.A.; Crisp, Ryan W.; Lauth, Jannika

DOI
10.1021/acs.jpclett.0c03461

Publication date
2021

Document Version
Final published version

Published in
Journal of Physical Chemistry Letters

Citation (APA)
Manteiga Vázquez, F., Yu, Q., Klepzig, L. F., Siebbeles, L. D. A., Crisp, R. W., & Lauth, J. (2021). Probing Excitons in Ultrathin PbS Nanoplatelets with Enhanced Near-Infrared Emission. *Journal of Physical Chemistry Letters*, *12*(1), 680-685. https://doi.org/10.1021/acs.jpclett.0c03461

THE JOURNAL OF PHYSICAL CHEMISTRY LETTERS
A JOURNAL OF THE AMERICAN CHEMICAL SOCIETY

pubs.acs.org/JPCL Letter

Probing Excitons in Ultrathin PbS Nanoplatelets with Enhanced Near-Infrared Emission

Francisco Manteiga Vázquez, Qianli Yu, Lars F. Klepzig, Laurens D. A. Siebbeles, Ryan W. Crisp, and Jannika Lauth*

Cite This: *J. Phys. Chem. Lett.* 2021, 12, 680−685 Read Online

ABSTRACT: Colloidal PbS nanoplatelets (NPLs) are highly interesting materials for near-infrared optoelectronic applications. We use ultrafast transient optical absorption spectroscopy to study the characteristics and dynamics of photoexcited excitons in ultrathin PbS NPLs with a cubic crystal structure. NPLs are synthesized at near room temperature from lead oleate and thiourea precursors; they show an optical absorption onset at 680 nm (1.8 eV) and photoluminescence at 720 nm (1.7 eV). By postsynthetically treating PbS NPLs with $CdCl_2$, their photoluminescence quantum yield is strongly enhanced from 1.4% to 19.4%. The surface treatment leads to an increased lead to sulfur ratio in the structures and associated reduced nonradiative recombination. Additionally, exciton−phonon interactions in pristine and $CdCl_2$ treated NPLs at frequencies of 1.96 and 2.04 THz are apparent from coherent oscillations in the transient absorption spectra. This study is an important step forward in unraveling and controlling the optical properties of IV−VI semiconductor NPLs.

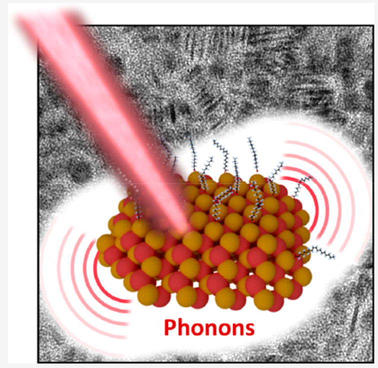

Ultrathin 2D colloidal semiconductor nanosheets (NSs) and nanoplatelets (NPLs) are highly topical materials with interesting optoelectronic properties strongly different from their spherical nanocrystal (NC) or solid-state counterparts. In contrast to II−VI semiconductor NPLs (e.g., CdSe) exhibiting strong absorption and photoluminescence (PL) in the visible range,[1−3] IV−VI semiconductors are of interest due to their widely tunable band gap and photoluminescence from the far-infrared to the near-infrared (NIR) by variation of the thickness of the NSs.[4,5] Covering the NIR range is crucial for advancing the spectral window inaccessible by CdSe-based NPLs without additional treatment including doping[6,7] or shell-growth.[6,8] In addition, exciton binding energies and charge carrier mobilities in 2D PbS can also be tuned by the thickness of the NSs. For example, thin PbS NSs exhibit stable excitons with high binding energies (~70 meV for 4 nm thickness) and carrier multiplication (CM) efficiencies approaching 100%, meaning that all photons with an energy exceeding the CM threshold generate additional electron−hole pairs.[9−11] Charge carrier mobilities increase with the thickness of the PbS NSs and become as high as 1000 $cm^2/(V\ s)$ for 16 nm thick NSs, which is close to the bulk mobility of PbS, while absorbing more light at longer wavelengths than thin NSs. Typically, PbS NSs with lateral dimensions of several micrometers and a thickness in the range of 4−40 nm are obtained by synthesis methods based on oriented attachment.[12−14] Recently, new colloidal synthesis methods for further decreasing the thickness of 2D PbS layers down to atomically thin PbS NPLs have been implemented, including a combination of surface ligand stabilization[15] as well as kinetically controlled reaction conditions.[16,17] These methods yield ultrathin 2D PbS layers with controllable lateral size as reaction product.[15,18,19] For example, ultrathin (1−2 nm) PbS NPLs were synthesized using the single-source precursor lead thiocyanate, and yielded NPLs with an orthorhombic crystal structure and high photoconductivity,[19] while the absorption of PbS NPLs synthesized from lead octadecylxanthate was optically tuned, albeit showing weak NIR PL.[20]

In this work, we elucidate the characteristics and dynamics of photoexcited electronic states (excitons) in ultrathin PbS NPLs by using ultrafast transient optical absorption spectroscopy. We study cubic rock-salt phase PbS NPLs obtained by a near room temperature synthesis method using lead oleate and thiourea precursors (see Scheme 1, Figure 1, and Figure S1 and the experimental part in the Supporting Information). Synthesis conditions are chosen following Hendricks et al.[21] such that pure lead oleate is used, instead of producing it *in situ* from oleic acid and lead acetate.[15,22] The procedure of presynthesizing lead oleate for the reaction is necessary to obtain the best results in terms of PbS NPL shape, size, and optical properties (see Figure 1, Figures S1 and S6). The reaction is carried out in octylamine with oleic acid and thiourea as the sulfur precursor. Exploiting an acid−base

Received: November 20, 2020
Accepted: December 28, 2020
Published: January 4, 2021

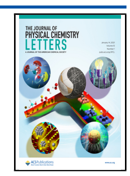

https://dx.doi.org/10.1021/acs.jpclett.0c03461
J. Phys. Chem. Lett. 2021, 12, 680−685

Scheme 1. Schematic of PbS NPLs Stacked on Edge and Lying Flat As Observed in the TEM Images Shown in Figure 1A

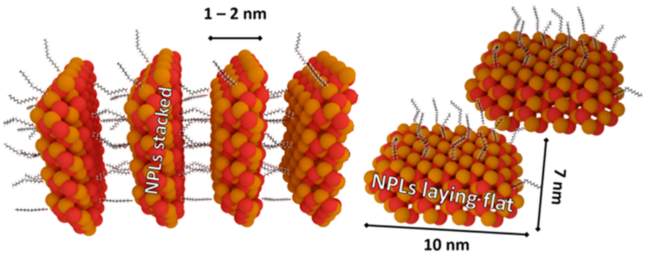

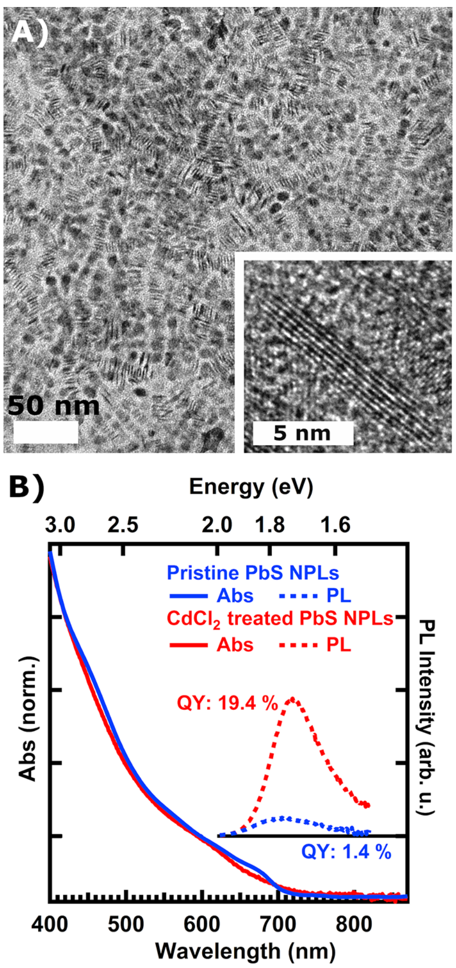

Figure 1. (A) TEM images of ultrathin PbS NPLs with lateral dimensions of 7×10 nm^2 and a thickness of 1−2 nm. Some NPLs are stacking on edge as shown in Scheme 1. The inset shows a single NPL on its edge. (B) Steady-state absorption and PL spectra of pristine PbS NPLs (blue) and after treatment with $CdCl_2$ (red), showing the absorption onset of the pristine NPLs at 680 nm (1.8 eV) and PL centered at 720 nm (1.7 eV) and broad absorption of the $CdCl_2$ treated sample with a slight rise near 620 nm (2.0 eV). The photoluminescence quantum yield of $CdCl_2$ treated PbS NPLs reaches 19.4%.

equilibrium between octylamine and oleic acid, which leads to the formation of an ammonium (RNH_3^+) species that supports the growth of 2D NPLs,[23] we obtain slightly elongated 2D PbS NPLs with a width of 7 nm and a length of 10 nm (see Figure 1A, Figure S1, and Scheme 1). The NPLs exhibit an absorption edge at 680 nm (1.8 eV) and NIR PL at 720 nm (1.7 eV) with a QY of 1.4% (see Figure 1B).

The obtained NPLs show the typical reflexes of the cubic PbS crystal system (see Figures S2 and S3 for powder XRD and SAED transmission electron microscopy rotational scans of the samples). EDS analysis yields a stoichiometric ratio of 1.1:1 for Pb:S in pristine NPL samples. In a postsynthetic step, the photoluminescence quantum yield (PLQY) of pristine PbS NPLs is increased to 19.4% by treating the crude reaction product with a $CdCl_2$ solution in octylamine (see the Supporting Information). Recently, Christodoulou et al. reported an increase in the thickness of CdSe NPLs after treating the samples with $CdCl_2$ with which the authors obtained CdSe NPLs with a thickness inaccessible under typical reaction conditions.[3] Generally, the surface treatment of NCs with metal halides leads to their stabilization and increase of their size.[24−28] In our case, after treating the pristine NPLs with $CdCl_2$, we find PbS layers with a slight regularity loss (see Figure S4) and an increased Pb:S ratio of 1.8:1 following EDS analysis, which resembles a lead rich surface typically found for PbS NCs.[29] A higher Pb:S ratio in $CdCl_2$ treated samples suggests the addition of Pb to the surface and/or edges of the NPLs, which is a reconstruction effect, as reported for CdSe NPLs[30] and NCs.[31] The lack of a significant absorption shift to shorter wavelengths (see Figure 1) and a Cd:Cl atomic ratio of 1:2 in $CdCl_2$ treated samples (see Figure S5 and Table S1) further excludes the growth of a CdS shell on the PbS NPLs or cation exchange which is, e.g., observed in PbS NC samples.[32] Figure 2 shows the Jacobian wavelength to energy converted

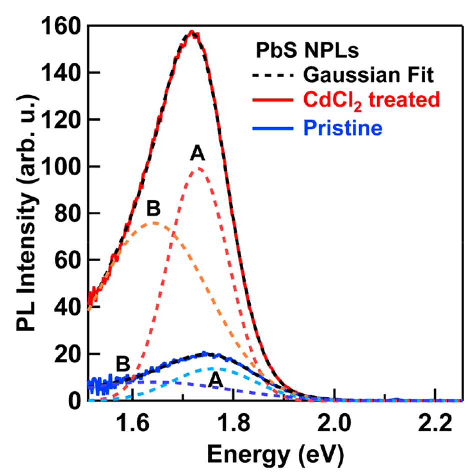

Figure 2. PL spectra of pristine (blue trace) and $CdCl_2$ treated (red trace) PbS NPLs. The emission is fit with a sum of two Gaussians (black dashed traces) with the two corresponding components A and B shown in lighter dashed lines.

steady-state PL spectra of pristine and $CdCl_2$ treated PbS NPLs in more detail.[33] Generally, PbS NCs exhibit a rather broad PL at room temperature, which was attributed to two emissive states in the NCs by Caram et al.[34] The authors ascribe PL from the PbS NC band edge as well as PL from an emissive "pinned" trap state in NCs to be responsible for PL line width broadening. Indeed, we find PbS NPL PL spectra are best fitted with the sum of two Gaussians (see Figure 2 and the fit function in the Supporting Information) for pristine and $CdCl_2$ treated samples.

Prior to the $CdCl_2$ treatment, PbS NPLs exhibit a band gap associated PL peak labeled A at 1.76 eV (705 nm) with a fwhm

https://dx.doi.org/10.1021/acs.jpclett.0c03461
J. Phys. Chem. Lett. 2021, 12, 680−685

of 192 meV (see Table 1 and Figure 2). After the treatment, the PL peak A at 1.73 eV (717 nm) shows a decreased fwhm of 142 meV. The "pinned" trap state associated peak labeled B stays fixed prior to and after the $CdCl_2$ treatment at 1.64 eV (756 nm). Both PL contributions A and B are strongly enhanced (albeit with an increasing contribution of B) after the $CdCl_2$ treatment, rendering it effective in increasing the overall PLQY of PbS NPLs.

Table 1. Values for the Two Gaussian Fits of the PbS NPL PL

	peak center (eV)		fwhm (meV)		peak area		peak ratio
PbS NPLs	A	B	peak A	peak B	A	B	A:B
pristine	1.76	1.64	192	356	2.80	3.03	0.93
$CdCl_2$ treated	1.73	1.64	142	260	15.0	21.0	0.72

As shown in Figure 1, $CdCl_2$ treated PbS NPLs exhibit a smaller absorption strength at 680 nm (1.8 eV) than pristine PbS NPLs and a slight rise in absorption near 620 nm (2.0 eV).

To further characterize the nature and dynamics of photoexcited states in pristine and $CdCl_2$ treated PbS NPLs, we apply ultrafast transient optical absorption (TA) spectroscopy as described in refs.[35−38] and briefly in the Supporting Information. The samples are photoexcited close to the band edge at 700 nm (with an optical density of ≤0.1) to prevent dynamic effects by charge carrier cooling and with the same photoexcitation density (2.5×10^{13} photons/cm^2) so that the distribution of the number of excitons in both NPL samples is similar.

The shape of the TA spectra in Figure 3 is discussed below on the basis of the terminology of electronic transitions and exciton states obtained from TA studies on PbSe[37,39] and PbS NCs.[36,40] Figure 3A,C shows 2D color-coded contour TA spectra of pristine and $CdCl_2$ treated PbS NPLs for comparison. The TA spectrum of pristine PbS NPLs exhibits a prominent negative ground-state (gs) bleach feature (1) of the $1S_h-1S_e$ transition at 673 nm due to state filling and stimulated emission, also observed in the spectral line cuts in Figure 3B. The maximum of gs bleach 1 is slightly blue-shifted with respect to the steady-state absorption at 680 nm (see Figure 1) implying a red shift in the excited-state absorption due to the formation of biexcitons by the probe pulse.[39] The small bleach feature (2) originates from the formally forbidden $1S_h-1P_e/1P_h-1S_e$ transitions that become slightly allowed in NCs due to symmetry breaking.[39,41] At shorter wavelengths, we probe the derivative-like feature (3) that we attribute to a red shift of the $1P_h-1P_e$ transition superimposed on a red-shifted ground-state absorption due to biexciton interactions.[42−44] We probe a wavelength-independent broad induced absorption at sub-band gap energies persisting over the TA time range studied (2.7 ns). This can be due to photoexcitation of trapped charges and/or due to further excitation of an exciton by the probe pulse, leading to intraband transitions.[45,46] The TA spectra of $CdCl_2$ treated PbS NPLs are very different from those of the pristine NPLs. Strikingly, they show two bleach features ((1a) and (2a)) at 677 and 613 nm with similar amplitudes and a long lifetime exceeding 3 ns (see Figure 3C,D). Since both bleach features are present for

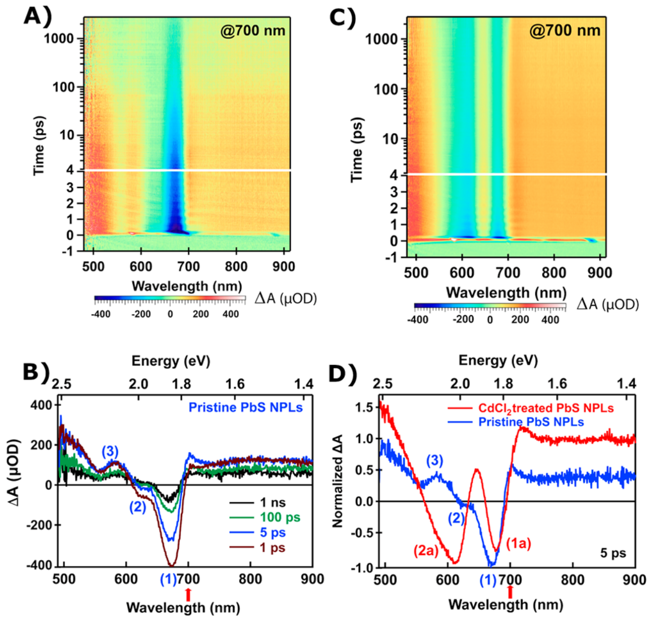

Figure 3. Color-coded 2D TA spectra of PbS NPLs photoexcited at 700 nm. (A) Pristine PbS NPLs exhibit one prominent bleach feature (1) at 673 nm. Additional features (2) and (3) and spectral line cuts at different times after photoexcitation are plotted in (B) and discussed in the text. (C) $CdCl_2$ treated NPLs show a strong effect of the treatment. (D) includes spectral line cuts taken from (A) and (C) at a delay time of 5 ps after photoexcitation, with $CdCl_2$ treated samples showing two prominent bleach features at 677 nm (1a) and 613 nm (2a). TA spectra are very distinct due to the involvement of different electronic states in the two samples as discussed in the text.

photoexcitation at a substantially longer wavelength (700 nm) than bleach feature (2a) at 613 nm, we exclude the latter being caused due to band edge excitons of thinner PbS NPLs after the $CdCl_2$ treatment. The strong bleach feature (2a) must be due to an additional electronic state introduced by the $CdCl_2$ treatment. In addition, the $CdCl_2$ treated PbS NPLs exhibit an increased induced absorption between features (1a) and (2a) and a stronger sub-band gap trap state and intraband absorption.[45]

Figure 4 includes the decay dynamics of the TA signal probed at the highest amplitude of the different bleach features for pristine and $CdCl_2$ treated PbS NPLs observed in Figure 3. The normalized decays show that bleach features (1a) and (2a) level off at approximately 20% of the original signal intensity after 20 ps, while bleach feature (1) decays over the time range of the measurement (15% of the original signal intensity after 20 ps and 5% after 2.7 ns). The larger bleach at long times in $CdCl_2$ treated PbS NPLs agrees well with the higher QY found in the samples.

Interestingly, we probe coherent oscillations in the TA spectra of PbS NPLs at short times after photoexcitation, as shown in the inset of Figure 4. Fourier transformation and a Lorentzian fit to the data of the short-time decay curve residuals yields frequencies of 1.96 THz (8.1 meV, 65.4 cm^{-1}) for pristine and 2.04 THz (8.4 meV, 68.1 cm^{-1}) for $CdCl_2$ treated NPLs (see Figure S7 and S8). These values correspond well with exciton−phonon coupling in pristine and $CdCl_2$ treated PbS NPLs to bulk-like optical and/or acoustic phonon modes of PbS at 1.96 THz (8.1 meV, 66 cm^{-1}) and 2.1 THz (8.4 meV, 68 cm^{-1}) respectively.[47−50]

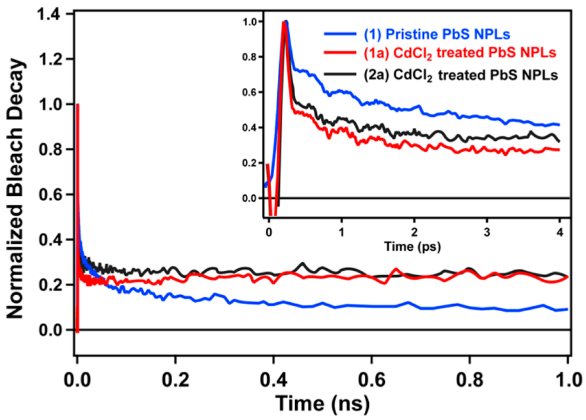

Figure 4. Decay dynamics of bleach features (1) of pristine and (1a) (red) and (2a) (black) of $CdCl_2$ treated PbS NPLs with transients for pristine NPLs decaying over the course of the measurement and with $CdCl_2$ treated sample transients leveling off at 20% of the original signal strength. The inset shows coherent oscillations originating from exciton−phonon interactions in PbS NPLs.

In conclusion, we have studied the optical properties of strongly quantum-confined colloidal cubic 2D PbS NPLs synthesized at near room temperature by steady-state PL and ultrafast TA spectroscopy for the first time. A new synthesis as well as a postsynthetic treatment of the obtained PbS NPLs with $CdCl_2$ increases their lead to sulfur ratio and leads to a strongly enhanced PLQY of 19.4%. Additionally, coherent oscillations probed by TA originate from strong exciton−phonon interactions in PbS NPLs. Our results render the surface treatment as a valuable tool for tuning the optical properties of PbS NPLs for near-infrared emission.

■ ASSOCIATED CONTENT

Supporting Information

The Supporting Information is available free of charge at https://pubs.acs.org/doi/10.1021/acs.jpclett.0c03461.

Synthesis of PbS NPLs, additional TEM images, XRD, instensity profiles, EDS spectra, elemental analysis, PLQY analysis, and brief description of the TA spectroscopic measurements (PDF)

■ AUTHOR INFORMATION

Corresponding Author

Jannika Lauth − *Institute of Physical Chemistry and Electrochemistry, Leibniz Universität Hannover, D-30167 Hannover, Germany; Cluster of Excellence PhoenixD (Photonics, Optics, and Engineering – Innovation Across Disciplines), D-30167 Hannover, Germany; Chemical Engineering Department, Delft University of Technology, 2629 HZ Delft, The Netherlands;* orcid.org/0000-0002-6054-9615; Email: jannika.lauth@pci.uni-hannover.de

Authors

Francisco Manteiga Vázquez − *Chemical Engineering Department, Delft University of Technology, 2629 HZ Delft, The Netherlands*

Qianli Yu − *Chemical Engineering Department, Delft University of Technology, 2629 HZ Delft, The Netherlands*

Lars F. Klepzig − *Institute of Physical Chemistry and Electrochemistry, Leibniz Universität Hannover, D-30167 Hannover, Germany; Cluster of Excellence PhoenixD (Photonics, Optics, and Engineering – Innovation Across Disciplines), D-30167 Hannover, Germany*

Laurens D. A. Siebbeles − *Chemical Engineering Department, Delft University of Technology, 2629 HZ Delft, The Netherlands;* orcid.org/0000-0002-4812-7495

Ryan W. Crisp − *Chemical Engineering Department, Delft University of Technology, 2629 HZ Delft, The Netherlands; Chemistry of Thin Film Materials, Department of Chemistry and Pharmacy, Friedrich-Alexander University Erlangen-Nürnberg, D-91058 Erlangen, Germany;* orcid.org/0000-0002-3703-9617

Complete contact information is available at: https://pubs.acs.org/10.1021/acs.jpclett.0c03461

Notes

The authors declare no competing financial interest.

■ ACKNOWLEDGMENTS

L.F.K. and J.L. greatly acknowledge funding by the Deutsche Forschungsgemeinschaft (DFG, German Research Foundation) under Germany's Excellence Strategy within the Cluster of Excellence PhoenixD (EXC 2122, Project ID 390833453). J.L. is thankful for funding by the Caroline Herschel program of the Leibniz Universität Hannover. We thank the Core Facility "Electron Microscopy" at the Universität Oldenburg for access to a HR-TEM JEOL JEM FS2100 instrument. PD Dr. Erhard Rhiel and Prof. Dr. Katharina Al-Shamery are acknowledged for their continuous support. Prof. Dr. Jürgen Caro and Prof. Dr. Armin Feldhoff are greatly acknowledged for the opportunity to perform XRD in their group.

■ REFERENCES

(1) Ithurria, S.; Tessier, M. D.; Mahler, B.; Lobo, R. P. S. M.; Dubertret, B.; Efros, A. L. Colloidal Nanoplatelets with Two-dimensional Electronic Structure. *Nat. Mater.* **2011**, *10*, 936−941.

(2) Ithurria, S.; Bousquet, G.; Dubertret, B. Continuous Transition from 3D to 1D Confinement Observed during the Formation of CdSe Nanoplatelets. *J. Am. Chem. Soc.* **2011**, *133*, 3070−3077.

(3) Christodoulou, S.; Climente, J. I.; Planelles, J.; Brescia, R.; Prato, M.; Martin-Garcia, B.; Khan, A. H.; Moreels, I. Chloride-Induced Thickness Control in CdSe Nanoplatelets. *Nano Lett.* **2018**, *18*, 6248−6254.

(4) Jiang, Z.; Bhandari, G. B.; Premathilaka, S. M.; Khan, S.; Dimick, D. M.; Stombaugh, C.; Mandell, A.; He, Y.; Peter Lu, H.; Sun, L. Growth of Colloidal PbS Nanosheets and the Enhancement of their Photoluminescence. *Phys. Chem. Chem. Phys.* **2015**, *17*, 23303−23307.

(5) Antu, A. D.; Jiang, Z.; Premathilka, S. M.; Tang, Y.; Hu, J.; Roy, A.; Sun, L. Bright Colloidal PbS Nanoribbons. *Chem. Mater.* **2018**, *30*, 3697−3703.

(6) Khan, A. H.; Pinchetti, V.; Tanghe, I.; Dang, Z.; Martín-García, B.; Hens, Z.; Van Thourhout, D.; Geiregat, P.; Brovelli, S.; Moreels, I. Tunable and Efficient Red to Near-Infrared Photoluminescence by Synergistic Exploitation of Core and Surface Silver Doping of CdSe Nanoplatelets. *Chem. Mater.* **2019**, *31*, 1450−1459.

(7) Galle, T.; Kazes, M.; Hübner, R.; Lox, J.; Samadi Khoshkhoo, M.; Sonntag, L.; Tietze, R.; Sayevich, V.; Oron, D.; Koitzsch, A.; et al. Colloidal Mercury-Doped CdSe Nanoplatelets with Dual Fluorescence. *Chem. Mater.* **2019**, *31* (14), 5065−5074.

(8) She, C.; Fedin, I.; Dolzhnikov, D. S.; Dahlberg, P. D.; Engel, G. S.; Schaller, R. D.; Talapin, D. V. Red, Yellow, Green, and Blue Amplified Spontaneous Emission and Lasing Using Colloidal CdSe Nanoplatelets. *ACS Nano* **2015**, *9*, 9475−9485.

(9) Lauth, J.; Failla, M.; Klein, E.; Klinke, C.; Kinge, S.; Siebbeles, L. D. A. Photoexcitation of PbS Nanosheets Leads to Highly Mobile

Charge Carriers and Stable Excitons. *Nanoscale* **2019**, *11*, 21569−21576.
(10) Aerts, M.; Bielewicz, T.; Klinke, C.; Grozema, F. C.; Houtepen, A. J.; Schins, J. M.; Siebbeles, L. D. A. Highly Efficient Carrier Multiplication in PbS Nanosheets. *Nat. Commun.* **2014**, *5*, 3789.
(11) Steiner, A. M.; Lissel, F.; Fery, A.; Lauth, J.; Scheele, M. Prospects of Coupled Organic-Inorganic Nanostructures for Charge and Energy Transfer Applications. *Angew. Chem., Int. Ed.* **2020**, DOI: 10.1002/anie.201916402.
(12) Schliehe, C.; Juarez, B. H.; Pelletier, M.; Jander, S.; Greshnykh, D.; Nagel, M.; Meyer, A.; Foerster, S.; Kornowski, A.; Klinke, C.; et al. Ultrathin PbS Sheets by Two-Dimensional Oriented Attachment. *Science* **2010**, *329*, 550−553.
(13) Bielewicz, T.; Ramin Moayed, M. M.; Lebedeva, V.; Strelow, C.; Rieckmann, A.; Klinke, C. From Dots to Stripes to Sheets: Shape Control of Lead Sulfide Nanostructures. *Chem. Mater.* **2015**, *27*, 8248−8254.
(14) Bielewicz, T.; Dogan, S.; Klinke, C. Tailoring the Height of Ultrathin PbS Nanosheets and Their Application as Field-Effect Transistors. *Small* **2015**, *11*, 826−833.
(15) Morrison, P. J.; Loomis, R. A.; Buhro, W. E. Synthesis and Growth Mechanism of Lead Sulfide Quantum Platelets in Lamellar Mesophase Templates. *Chem. Mater.* **2014**, *26*, 5012−5019.
(16) Riedinger, A.; Ott, F. D.; Mule, A.; Mazzotti, S.; Knusel, P. N.; Kress, S. J. P.; Prins, F.; Erwin, S. C.; Norris, D. J. An Intrinsic Growth Instability in Isotropic Materials leads to Quasi-Two-Dimensional Nanoplatelets. *Nat. Mater.* **2017**, *16*, 743.
(17) Ott, F. D.; Riedinger, A.; Ochsenbein, D. R.; Knüsel, P. N.; Erwin, S. C.; Mazzotti, M.; Norris, D. J. Ripening of Semiconductor Nanoplatelets. *Nano Lett.* **2017**, *17*, 6870−6877.
(18) Khan, A. H.; Pal, S.; Dalui, A.; Pradhan, J.; Sarma, D. D.; Acharya, S. Solution-Processed Free-Standing Ultrathin Two-Dimensional PbS Nanocrystals with Efficient and Highly Stable Dielectric Properties. *Chem. Mater.* **2017**, *29*, 1175−1182.
(19) Akkerman, Q. A.; Martín-García, B.; Buha, J.; Almeida, G.; Toso, S.; Marras, S.; Bonaccorso, F.; Petralanda, U.; Infante, I.; Manna, L. Ultrathin Orthorhombic PbS Nanosheets. *Chem. Mater.* **2019**, *31*, 8145−8153.
(20) Khan, A. H.; Brescia, R.; Polovitsyn, A.; Angeloni, I.; Martín-García, B.; Moreels, I. Near-Infrared Emitting Colloidal PbS Nanoplatelets: Lateral Size Control and Optical Spectroscopy. *Chem. Mater.* **2017**, *29*, 2883−2889.
(21) Hendricks, M. P.; Campos, M. P.; Cleveland, G. T.; Jen-La Plante, I.; Owen, J. S. A Tunable Library of Substituted Thiourea Precursors to Metal Sulfide Nanocrystals. *Science* **2015**, *348*, 1226−1230.
(22) Houtepen, A. J.; Koole, R.; Vanmaekelbergh, D.; Meeldijk, J.; Hickey, S. G. The Hidden Role of Acetate in the PbSe Nanocrystal Synthesis. *J. Am. Chem. Soc.* **2006**, *128*, 6792−6793.
(23) Almeida, G.; Goldoni, L.; Akkerman, Q.; Dang, Z.; Khan, A. H.; Marras, S.; Moreels, I.; Manna, L. Role of Acid−Base Equilibria in the Size, Shape, and Phase Control of Cesium Lead Bromide Nanocrystals. *ACS Nano* **2018**, *12*, 1704−1711.
(24) Zhang, J.; Gao, J.; Miller, E. M.; Luther, J. M.; Beard, M. C. Diffusion-Controlled Synthesis of PbS and PbSe Quantum Dots with in Situ Halide Passivation for Quantum Dot Solar Cells. *ACS Nano* **2014**, *8*, 614−622.
(25) Lim, J.; Bae, W. K.; Park, K. U.; zur Borg, L.; Zentel, R.; Lee, S.; Char, K. Controlled Synthesis of CdSe Tetrapods with High Morphological Uniformity by the Persistent Kinetic Growth and the Halide-Mediated Phase Transformation. *Chem. Mater.* **2013**, *25*, 1443−1449.
(26) Crisp, R. W.; Kroupa, D. M.; Marshall, A. R.; Miller, E. M.; Zhang, J.; Beard, M. C.; Luther, J. M. Metal Halide Solid-State Surface Treatment for High Efficiency PbS and PbSe QD Solar Cells. *Sci. Rep.* **2015**, *5*, 9945.
(27) Cho, W.; Kim, S.; Coropceanu, I.; Srivastava, V.; Diroll, B. T.; Hazarika, A.; Fedin, I.; Galli, G.; Schaller, R. D.; Talapin, D. V. Direct Synthesis of Six-Monolayer (1.9 nm) Thick Zinc-Blende CdSe Nanoplatelets Emitting at 585 nm. *Chem. Mater.* **2018**, *30*, 6957−6960.
(28) Meerbach, C.; Wu, C.; Erwin, S. C.; Dang, Z.; Prudnikau, A.; Lesnyak, V. Halide-Assisted Synthesis of Cadmium Chalcogenide Nanoplatelets. *Chem. Mater.* **2020**, *32*, 566−574.
(29) Weidman, M. C.; Beck, M. E.; Hoffman, R. S.; Prins, F.; Tisdale, W. A. Monodisperse, Air-Stable PbS Nanocrystals via Precursor Stoichiometry Control. *ACS Nano* **2014**, *8*, 6363−6371.
(30) Sun, H.; Buhro, W. E. Reversible Z-Type to L-Type Ligand Exchange on Zinc-Blende Cadmium Selenide Nanoplatelets. *Chem. Mater.* **2020**, *32*, 5814−5826.
(31) Marino, E.; Kodger, T. E.; Crisp, R. W.; Timmerman, D.; MacArthur, K. E.; Heggen, M.; Schall, P. Repairing Nanoparticle Surface Defects. *Angew. Chem., Int. Ed.* **2017**, *56*, 13795−13799.
(32) Zhang, J.; Chernomordik, B. D.; Crisp, R. W.; Kroupa, D. M.; Luther, J. M.; Miller, E. M.; Gao, J.; Beard, M. C. Preparation of Cd/Pb Chalcogenide Heterostructured Janus Particles via Controllable Cation Exchange. *ACS Nano* **2015**, *9*, 7151−7163.
(33) Mooney, J.; Kambhampati, P. Get the Basics Right: Jacobian Conversion of Wavelength and Energy Scales for Quantitative Analysis of Emission Spectra. *J. Phys. Chem. Lett.* **2013**, *4*, 3316−3318.
(34) Caram, J. R.; Bertram, S. N.; Utzat, H.; Hess, W. R.; Carr, J. A.; Bischof, T. S.; Beyler, A. P.; Wilson, M. W. B.; Bawendi, M. G. PbS Nanocrystal Emission Is Governed by Multiple Emissive States. *Nano Lett.* **2016**, *16*, 6070−6077.
(35) Lauth, J.; Kinge, S.; Siebbeles, L. D. A. Ultrafast Transient Absorption and Terahertz Spectroscopy as Tools to Probe Photoexcited States and Dynamics in Colloidal 2D Nanostructures. *Z. Phys. Chem.* **2017**, *231*, 107−119.
(36) Lauth, J.; Grimaldi, G.; Kinge, S.; Houtepen, A. J.; Siebbeles, L. D. A.; Scheele, M. Ultrafast Charge Transfer and Upconversion in Zn β-Tetraaminophthalocyanine Functionalized PbS Nanostructures Probed by Transient Absorption Spectroscopy. *Angew. Chem., Int. Ed.* **2017**, *56*, 14061−14065.
(37) Spoor, F. C. M.; Kunneman, L. T.; Evers, W. H.; Renaud, N.; Grozema, F. C.; Houtepen, A. J.; Siebbeles, L. D. A. Hole Cooling Is Much Faster than Electron Cooling in PbSe Quantum Dots. *ACS Nano* **2016**, *10*, 695−703.
(38) Kunneman, L. T.; Tessier, M. D.; Heuclin, H.; Dubertret, B.; Aulin, Y. V.; Grozema, F. C.; Schins, J. M.; Siebbeles, L. D. A. Bimolecular Auger Recombination of Electron−Hole Pairs in Two-Dimensional CdSe and CdSe/CdZnS Core/Shell Nanoplatelets. *J. Phys. Chem. Lett.* **2013**, *4*, 3574−3578.
(39) Schins, J. M.; Trinh, M. T.; Houtepen, A. J.; Siebbeles, L. D. A. Probing Formally Forbidden Optical Transitions in PbSe Nanocrystals by Time- and Energy-Resolved Transient Absorption Spectroscopy. *Phys. Rev. B: Condens. Matter Mater. Phys.* **2009**, *80*, 035323.
(40) Yang, Y.; Rodríguez-Córdoba, W.; Lian, T. Ultrafast Charge Separation and Recombination Dynamics in Lead Sulfide Quantum Dot−Methylene Blue Complexes Probed by Electron and Hole Intraband Transitions. *J. Am. Chem. Soc.* **2011**, *133*, 9246−9249.
(41) Trinh, M. T.; Houtepen, A. J.; Schins, J. M.; Piris, J.; Siebbeles, L. D. A. Nature of the Second Optical Transition in PbSe Nanocrystals. *Nano Lett.* **2008**, *8*, 2112−2117.
(42) Geiregat, P.; Houtepen, A.; Justo, Y.; Grozema, F. C.; Van Thourhout, D.; Hens, Z. Coulomb Shifts upon Exciton Addition to Photoexcited PbS Colloidal Quantum Dots. *J. Phys. Chem. C* **2014**, *118*, 22284−22290.
(43) Gdor, I.; Shapiro, A.; Yang, C.; Yanover, D.; Lifshitz, E.; Ruhman, S. Three-Pulse Femtosecond Spectroscopy of PbSe Nanocrystals: 1S Bleach Nonlinearity and Sub-Band-Edge Excited-State Absorption Assignment. *ACS Nano* **2015**, *9*, 2138−2147.
(44) Kambhampati, P. Unraveling the Structure and Dynamics of Excitons in Semiconductor Quantum Dots. *Acc. Chem. Res.* **2011**, *44*, 1−13.
(45) De Geyter, B.; Houtepen, A. J.; Carrillo, S.; Geiregat, P.; Gao, Y.; ten Cate, S.; Schins, J. M.; Van Thourhout, D.; Delerue, C.; Siebbeles, L. D. A.; et al. Broadband and Picosecond Intraband

Absorption in Lead-Based Colloidal Quantum Dots. *ACS Nano* **2012**, *6*, 6067−6074.
(46) An, J. M.; Franceschetti, A.; Dudiy, S. V.; Zunger, A. The Peculiar Electronic Structure of PbSe Quantum Dots. *Nano Lett.* **2006**, *6*, 2728−2735.
(47) Wang, H.; Lhuillier, E.; Yu, Q.; Mottaghizadeh, A.; Ulysse, C.; Zimmers, A.; Descamps-Mandine, A.; Dubertret, B.; Aubin, H. Effects of Electron-Phonon Interactions on the Electron Tunneling Spectrum of PbS Quantum Dots. *Phys. Rev. B: Condens. Matter Mater. Phys.* **2015**, *92*, 041403.
(48) Lead Sulfide (PbS) Phonon Dispersion and Frequencies: Datasheet from Landolt-Börnstein - Group III Condensed Matter. *Non-Tetrahedrally Bonded Elements and Binary Compounds I*; Madelung, O., Rössler, U., Schulz, M., Eds.; SpringerMaterials; Springer-Verlag: Berlin, Heidelberg, Germany, 1998; Vol. *41C*.
(49) Krauss, T. D.; Wise, F. W.; Tanner, D. B. Observation of Coupled Vibrational Modes of a Semiconductor Nanocrystal. *Phys. Rev. Lett.* **1996**, *76*, 1376−1379.
(50) Krauss, T. D.; Wise, F. W. Coherent Acoustic Phonons in a Semiconductor Quantum Dot. *Phys. Rev. Lett.* **1997**, *79*, 5102−5105.